AGU PUBLICATIONS

Geophysical Research Letters

RESEARCH LETTER
10.1002/2017GL073602

Key Points:
- 3-D structure and transport of a subglacial discharge plume from novel near-glacier surveying
- Observed plume is inconsistent with axisymmetric plume theory commonly used to model submarine melt and near-glacier circulation
- Observations point toward a wider plume that drives higher entrainment and more submarine melting

Supporting Information:
- Supporting Information S1

Correspondence to:
R. H. Jackson,
rjackson@coas.oregonstate.edu

Citation:
Jackson, R. H., E. L. Shroyer, J. D. Nash, D. A. Sutherland, D. Carroll, M. J. Fried, G. A. Catania, T. C. Bartholomaus, and L. A. Stearns (2017), Near-glacier surveying of a subglacial discharge plume: Implications for plume parameterizations, *Geophys. Res. Lett.*, *44*, 6886–6894, doi:10.1002/2017GL073602.

Received 24 MAR 2017
Accepted 13 JUN 2017
Accepted article online 15 JUN 2017
Published online 3 JUL 2017

Near-glacier surveying of a subglacial discharge plume: Implications for plume parameterizations

R. H. Jackson[1], E. L. Shroyer[1], J. D. Nash[1], D. A. Sutherland[2], D. Carroll[2], M. J. Fried[3,4], G. A. Catania[3,4], T. C. Bartholomaus[5], and L. A. Stearns[6]

[1]College of Earth, Ocean, and Atmospheric Sciences, Oregon State University, Corvallis, Oregon, USA, [2]Department of Earth Sciences, University of Oregon, Eugene, Oregon, USA, [3]Institute for Geophysics, University of Texas at Austin, Austin, Texas, USA, [4]Department of Geological Sciences, University of Texas at Austin, Austin, Texas, USA, [5]Department of Geography, University of Idaho, Moscow, Idaho, USA, [6]Department of Geology, University of Kansas, Lawrence, Kansas, USA

Abstract At tidewater glaciers, plume dynamics affect submarine melting, fjord circulation, and the mixing of meltwater. Models often rely on buoyant plume theory to parameterize plumes and submarine melting; however, these parameterizations are largely untested due to a dearth of near-glacier measurements. Here we present a high-resolution ocean survey by ship and remotely operated boat near the terminus of Kangerlussuup Sermia in west Greenland. These novel observations reveal the 3-D structure and transport of a near-surface plume, originating at a large undercut conduit in the glacier terminus, that is inconsistent with axisymmetric plume theory, the most common representation of plumes in ocean-glacier models. Instead, the observations suggest a wider upwelling plume—a "truncated" line plume of ~200 m width—with higher entrainment and plume-driven melt compared to the typical axisymmetric representation. Our results highlight the importance of a subglacial outlet's geometry in controlling plume dynamics, with implications for parameterizing the exchange flow and submarine melt in glacial fjord models.

1. Introduction

The subglacial discharge plumes that upwell along the termini of tidewater glaciers are hot spots of mixing between glacial freshwater and ocean waters. Entrainment into these plumes affects both the heat transfer for submarine melting and the mixing of freshwater as it is exported into the ocean.

Recent changes in the Greenland Ice Sheet have drawn increased attention to these heat and freshwater exchanges at outlet glaciers. The ice sheet is losing mass, contributing to roughly one quarter of current sea level rise [*Shepherd et al.*, 2012], and the ocean has been implicated as a potential trigger for glacier retreat [*Holland et al.*, 2008; *Motyka et al.*, 2011; *Straneo and Heimbach*, 2013]. The presumed connection between ocean warming and glacier retreat is enhanced submarine melting, yet submarine melting has not been directly measured at any glacier in Greenland.

Additionally, the total freshwater discharge from the ice sheet—runoff, submarine melt, and iceberg calving—is increasing [*Bamber et al.*, 2012; *Enderlin et al.*, 2014], with implications for the coastal and subpolar gyre-scale circulation [*Weijer et al.*, 2012; *Lenaerts et al.*, 2015]. The dilution of glacial freshwater by ambient ocean waters in upwelling plumes sets the properties of glacially modified waters before they are exported through fjords and onto the continental shelf. Previously observed glacial plume waters contain less than 10% freshwater [*Bendtsen et al.*, 2015; *Beaird et al.*, 2015; *Stevens et al.*, 2016; *Mankoff et al.*, 2016], indicating that the bulk of the dilution has already occurred in the upwelling plume before the horizontal outflow. However, no subsurface measurements have been obtained in the upwelling core, where mixing and plume-driven melting occur; instead, this region is exclusively the purview of models and theory.

In the absence of direct measurements, a variety of models have been used to study the ocean-glacier interface. At the core of almost all these models is buoyant plume theory (BPT), which describes the evolution of a plume for a given buoyancy forcing, stratification and geometry [*Morton et al.*, 1956; *Ellison and Turner*, 1959]. BPT has been applied to ice shelves and vertical termini, coupled with melt parameterizations, to model glacial plume entrainment and submarine melt [*MacAyeal*, 1985; *Holland and Jenkins*, 1999; *Jenkins*, 2011].

BPT is used not only to model glacial plumes directly [e.g., *Jenkins*, 2011; *Slater et al.*, 2016; *Carroll et al.*, 2016] but also to set a constant turbulent diffusivity in numerical models of glacial plumes [*Sciascia et al.*, 2013; *Kimura et al.*, 2014; *Carroll et al.*, 2015; *Slater et al.*, 2015, 2017a]. Other numerical modeling studies do not include the plumes explicitly but instead force their coarser-resolution models with BPT solutions [*Cowton et al.*, 2015, 2016]. Broadly, these theoretical and numerical models all show that submarine melting increases with ambient ocean temperature and with subglacial discharge—enhanced buoyancy forcing causes larger velocities at the ice-ocean interface and more effective heat transfer.

The net entrainment and submarine melting, however, are sensitive to the geometry of the plume and its entraining surface area [*Kimura et al.*, 2014; *Carroll et al.*, 2015; *Slater et al.*, 2015]. Two varieties of BPT have commonly been applied to represent different source geometries: a line plume configuration to model discharge distributed along the whole grounding line [*Jenkins*, 2011; *Sciascia et al.*, 2013] and an axisymmetric plume (also called a point or half-cone plume) to model discharge from a subglacial channel, assuming an outlet of O(10 m) width [*Kimura et al.*, 2014; *Cowton et al.*, 2015; *Carroll et al.*, 2016; *Bartholomaus et al.*, 2016]. However, without direct observations of subglacial channels/outlets or their upwelling plumes, the geometries used in these plume models are unvalidated.

At this time, observational validation of subglacial plume parameterizations is limited and without a general consensus. *Mankoff et al.* [2016] observed a plume's volume flux and water properties that were in relatively good agreement with axisymmetric BPT. Similarly, *Bartholomaus et al.* [2016] argued that the presence/absence of surface plumes is roughly consistent with axisymmetric BPT when forced with estimates of discharge. On the other hand, *Slater et al.* [2017a] used a similar approach as *Bartholomaus et al.* [2016] to argue that there must be more entrainment than axisymmetric BPT can predict. *Stevens et al.* [2016] observed water properties in two plume cores and showed that one was consistent with axisymmetric BPT while the other was not.

Here we use a high-resolution ocean survey to examine the 3-D structure and transport of a subglacial discharge plume. These novel measurements, which include 11 repeat sections across the outflowing plume, allow for a more robust comparison between observations and glacial plume parameterizations.

2. Setting and Data

2.1. KS Glacier-Fjord System

Kangerlussuup Sermia (KS) flows into the Uummannaq fjord system of west Greenland (Figure 1a) with an annual mean velocity of 4.9 m d^{-1} [*Bartholomaus et al.*, 2016]. The glacier terminus, which is 4.2 km wide, grounds on a broad morainal bank at 260 m depth [*Fried et al.*, 2015; *Bartholomaus et al.*, 2016]. Away from the glacier, the fjord is over 400 m deep, with no sill to impede the buoyancy-driven circulation from the glacier [*Bartholomaus et al.*, 2016].

Multibeam surveying of the terminus of KS in 2013 revealed multiple undercut outlets ($\sim$150 $\times$ 150 m with a backwall slope of $\sim$45°), the largest of which is located at the prow of the glacier and aligned with the main subglacial discharge pathway from subglacial flow path modeling (Figure 1a) [*Fried et al.*, 2015]. At the surface, sediment plumes regularly appear near the prow (diagnosed over 5 years of imagery), confirming the presence of a persistent subglacial channel outlet in this location [*Fried et al.*, 2015].

2.2. Data

Eleven repeat transects of line KS-1 (Figure 1), approximately 1.5 km from the glacier, were occupied over 26 h on 28–29 July 2014 as part of a larger 3 year field campaign (described in *Bartholomaus et al.* [2016]). A shipboard acoustic doppler current profiler (ADCP) recorded velocity from 6 to $\sim$160 m depth, and repeat profiling provided water properties (conductivity-temperature-depth, CTD) from 2 to 300 m depth. Simultaneously, a remotely operated boat (ROB) surveyed between 200 m and 1.6 km of the terminus, in the region of transect KS-0 (Figure 1a), recording velocity between 6 and 80 m depth with an ADCP and water properties between 2 and 120 m with a CTD. (Surveying details can be found in the supporting information.)

Further downstream, shipboard CTD and ADCP measurements were collected at KS-6 (15 km from the glacier) and outside the fjord in Uummannaq Bay (Figure 1a). Additionally, a mooring was deployed 6 km from the terminus for 10 months prior to the survey [*Bartholomaus et al.*, 2016]. On the mooring, an ADCP measured velocity from 74 to 424 m depth, providing deep velocities below the range of the ship's ADCP.

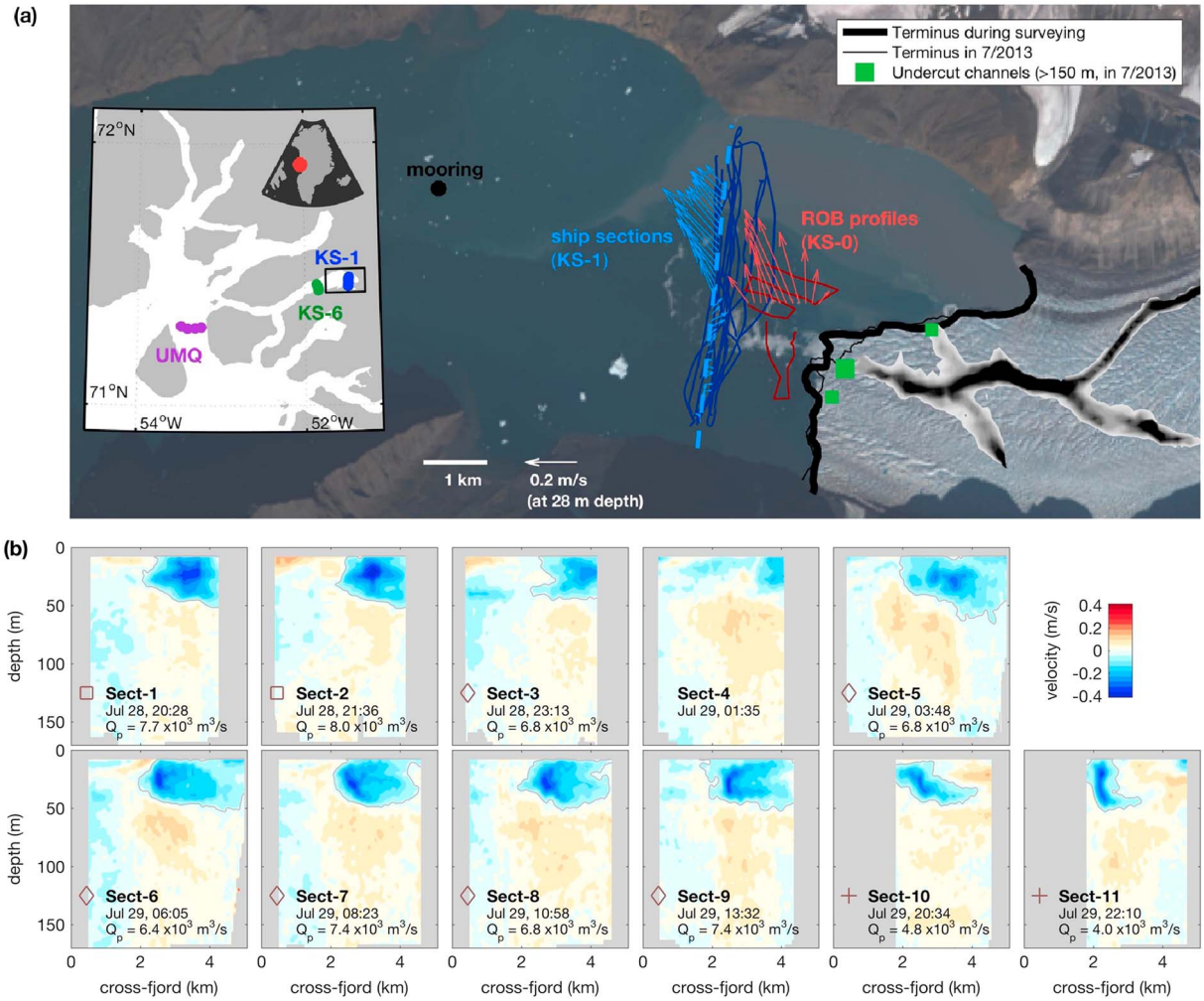

Figure 1. (a) Satellite image of near-glacier region with tracks of 11 repeat sections at KS-1 by ship (dark blue) and surveying around KS-0 by ROB (dark red). Vectors show velocity at 28 m depth from the second occupation of KS-1 (light blue) and ROB surveying at KS-0 (light red). The dashed blue line shows the transect orientation used in Figure 1b. The mooring location is shown with a black dot. Green squares indicate the location of undercut channels (>150 m) from a multibeam survey in July of 2013—the largest is found at the prow—and subglacial flow path probabilities are shown in grey scale over the glacier, with darker colors representing most likely subglacial channel locations [*Fried et al.*, 2015]. Inset: regional map with additional sections at 15 km from the glacier (KS-6) and outside the fjord in Uummannaq Bay (UMQ). (b) Eleven repeat sections of KS-1 over 26 h, showing component of velocity along principal axis, 35° west of north, with positive velocities toward the glacier. Symbols at the bottom of each subpanel are used to identify sections in Figure 3: squares are two sections with velocity but no CTD; crosses are the two sections at the end of surveying, separated by 7 h from other sections; Sect-4 has no symbol since the plume core is not well resolved; and the rest are diamonds. Thin grey lines are the −0.03 m s^{-1} contour that is used to define the plume and calculate its volume flux, Q_p.

Runoff over the KS catchment basin is estimated with RACMO2.3 output [*Noel et al.*, 2015; *Bartholomaus et al.*, 2016]. The average runoff over July–August 2014 is 230 m^3 s^{-1}, with a summer maximum of 540 m^3 s^{-1} (Figure S1 in the supporting information). These numbers, however, are only reported for general context, since both the routing/storage and the exact discharge distribution at the terminus are unknown.

3. Plume Structure and Transport

Eleven repeat sections at KS-1 show a persistent, subsurface plume flowing away from the glacier with peak speeds at 30 m depth (Figure 1b). Simultaneous surveying at KS-0 (500 m from the glacier) reveals a plume of similar structure, properties, and transport (Figure 2a). The plume's northwest trajectory bends slightly to the west between these sections and is consistent with the plume originating at the prow of the terminus (Figures 1a and S3). In a concurrent time-lapse video, a surface sediment pool is visible at the prow (supporting information), indicating that the plume likely overshot its neutral density before outflowing as a subsurface

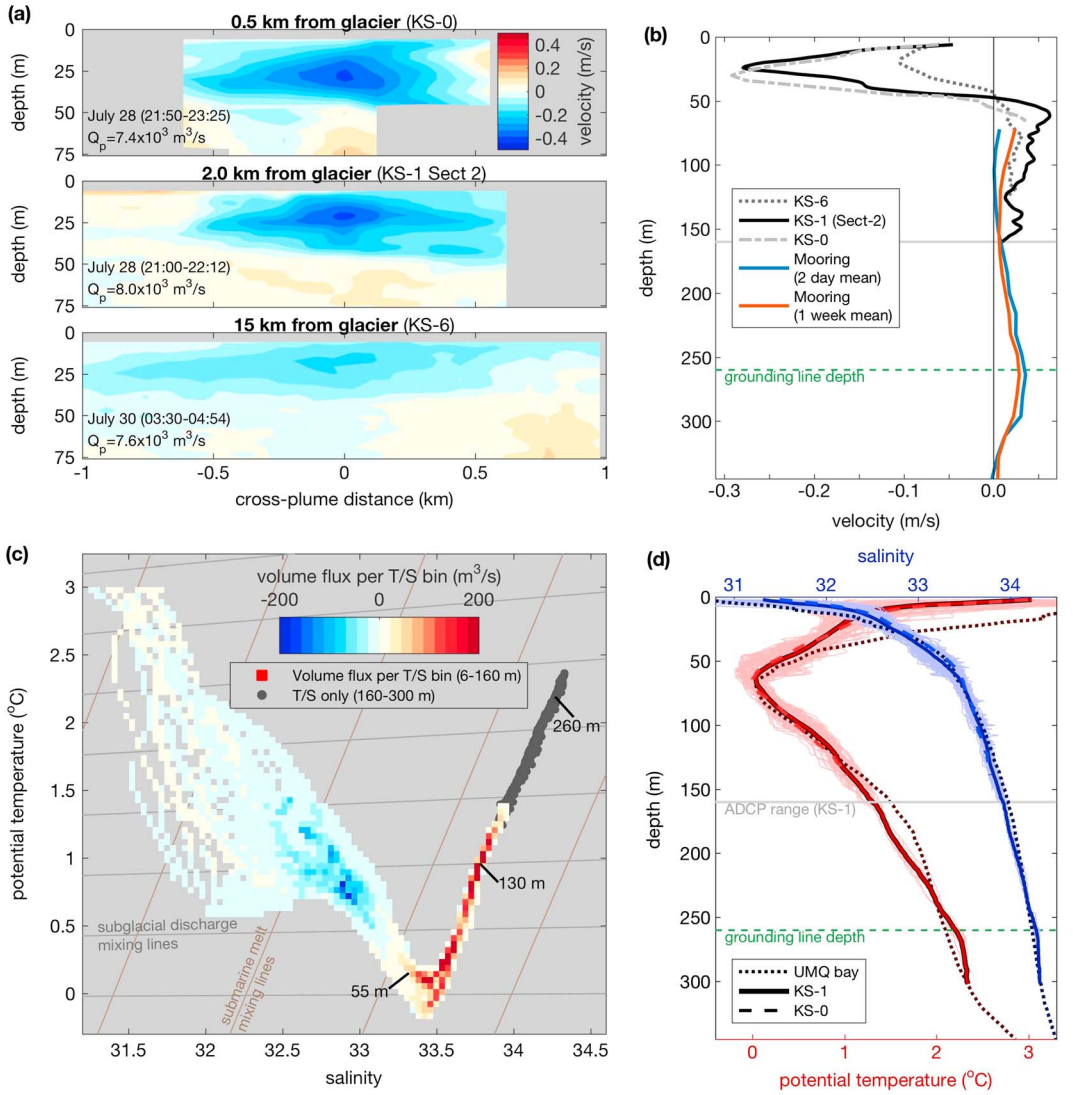

Figure 2. (a) Cross-plume sections at KS-0, KS-1 (Sect-2, overlapping in time with KS-0) and KS-6 (15 km from the glacier; 29 h after KS-0/1). The *x* axis is the cross-plume coordinate, perpendicular to maximum velocity (different than the cross-fjord coordinate in Figure 1b). Q_p is the plume's volume flux within the −0.03 m s^{-1} velocity contour. (b) Depth versus laterally averaged velocity from sections in Figure 2a. For KS-0 (light grey dashed) and KS-1 (black), velocity is laterally averaged over ±0.5 km of the maximum velocity; for KS-6 (grey dashed), velocity is averaged over ±1 km of the maximum velocity. Along-fjord velocities from the mooring are averaged over 2 days (blue) and 1 week (red) preceding the survey. Negative velocities are away from the glacier. (c) In color: average volume flux per T/S bin from KS-1 sections over the ADCP depth range of 6–160 m. Grey dots are T/S properties from 160 to 300 m, also at KS-1. Subglacial discharge mixing lines (assuming discharge of $S = 0$, $T = -0.2$°C) are in light grey and submarine melt mixing lines (assuming $S = 0$ and an effective temperature of −90°C) [*Gade*, 1979] in brown. (d) Potential temperature and salinity versus depth. Thick dashed, solid, and dotted lines show averages from KS-0, KS-1, and outside the fjord in Uummannaq Bay (UMQ), respectively. Thin lines show all CTD casts from KS-1.

plume at KS-0. Further downstream at KS-6, velocities are weaker and the plume has spread laterally, doubling its width (Figures 2a and 2b).

At KS-1, there is a weak inflow toward the glacier below ~50 m (<0.05 m s^{-1}; Figure 1b). The deep inflow is only partially resolved in shipboard measurements; the mean along-fjord velocity from the mooring shows additional flow toward the glacier below 150 m and a peak inflow near the glacier's grounding line depth (Figure 2b).

The primary water masses near the glacier are similar to those found in Uummannaq Bay: warm, Atlantic-origin water at depth, a polar-origin temperature minimum at ~70 m, and warm, fresh surface water

(Figure 2d). The volume flux binned by temperature/salinity (T/S) in Figure 2c shows that the outflowing plume properties are concentrated in a small part of T/S space, centered at 32.8 practical salinity unit (psu) and 0.9°C, that is consistent with subglacial discharge mixing with and then upwelling deeper waters. However, the water properties in the plume are not a significant anomaly relative to the adjacent water at the same depth. With T/S properties alone, one could not "tag" the plume as glacially modified water; velocity measurements are key to identifying and examining the outflow plume. Isopycnals bulge slightly around the outflowing core, with a stratification minimum in the plume (Figure S3).

While the outflow is concentrated in a small part of T/S space, the deep inflow toward the glacier transports a wide range of water properties, including Atlantic-origin water, that match the deep water column in Uummannaq Bay (Figures 2c and 2d).

The repeat KS-1 sections provide 10 independent realizations of the outflowing plume and its volume transport (omitting Sect-4 where the plume core is not well resolved). The average plume volume flux, calculated by integrating the transport within the -0.03 m s^{-1} contour that encloses the peak outflowing velocity (Figure 1b), is 6600 m^3 s^{-1} with a standard deviation of 1300 m^3 s^{-1} (supporting information). The plume signal is persistent but variable in structure and transport. In particular, Sect-10 and Sect-11, which were occupied 7 h after Sect-9, show a plume with a narrower core, stronger lateral shear, and lower volume flux relative to the other sections.

Without fully resolving the deep inflow and the mean water properties that are entrained into the plume, we cannot definitively assess the fraction of subglacial discharge or submarine melt in the plume. We can, however, constrain the plume to have $< 4.4 \pm 0.2\%$ total freshwater. Combined with the plume's volume flux, this gives an upper bound of 260 ± 70 m^3 s^{-1} freshwater feeding the plume. If we assume that all entrainment occurs below 55 m (i.e., the plume entrains only waters with a linear T/S relationship in Figure 2c), the subglacial discharge flux can be estimated as 190 ± 50 m^3 s^{-1}. Details and caveats of these estimates are discussed in the supporting information [*Jenkins*, 1999; *Motyka et al.*, 2003; *Jackson and Straneo*, 2016].

Between KS-0 and KS-1, the plume's volume flux does not change significantly (7400 ± 300 m^3 s^{-1} at KS-0 versus 8000 ± 200 m^3 s^{-1} at KS-1 Sect-2; Figure 2a), and there is no clear difference in properties or stratification (Figure 2d). Together, this suggests that the entrainment in the observed portion of the outflowing plume is insignificant compared to the prior entrainment that created a plume of >7000 m^3 s^{-1} from <260 m^3 s^{-1} of freshwater—a dilution ratio of at least 26 [e.g., *Carroll et al.*, 2016]. Further downstream at KS-6, the outflow has a similar transport of 7600 ± 400 m^3 s^{-1} (though KS-6 was occupied 29 h after the KS-0/1 sections).

4. Comparing Observations With Plume Theory

We compare the observed plume's volume flux and water properties to idealized buoyant plume theory (BPT) in both line and axisymmetric geometries. In addition to the standard configurations—axisymmetric plumes for channelized discharge and line plumes for discharge distributed across the whole terminus—we also consider "truncated" line plumes with widths that vary from 100 m (approximately the lower limit for line plume theory to be valid; see supporting information) to the full terminus width.

We use line plume theory from *Jenkins* [2011] and axisymmetric theory for a half-cone shape from *Cowton et al.* [2015]. For both geometries, the plume's evolution is solved using conservation equations for volume, momentum, heat, and salt with a submarine melt parameterization from the three-equation formulation in *Holland and Jenkins* [1999]. The plume is initialized assuming a balance of buoyancy and momentum, solved with an entrainment coefficient of $\alpha = 0.1 \pm 0.01$ [*Morton et al.*, 1956], and all other parameters have values following *Jenkins* [2011]. The subglacial discharge enters at the grounding line depth (260 ± 10 m) and the ambient ocean stratification is set by the mean stratification measured at KS-1. We use a range of subglacial discharge fluxes between 20 and 500 m^3 s^{-1}, an upper limit from RACMO2.3 runoff. We assume a vertical calving front because the effects of ice slope should be negligible for the range of ice slopes and discharge fluxes in question [*Jenkins*, 2011; *Slater et al.*, 2017b]. (See supporting information for BPT details.)

The BPT integration is stopped when the plume's momentum is zero, or if the plume reaches the surface, and these terminal properties are compared to the KS observations. Thus, we are comparing the terminal properties predicted by BPT for the *upwelling* portion of the plume with the observed *outflowing* plume at 0.5 km (and greater distances) from the glacier. Any additional entrainment as the plume transitions from upwelling to outflowing is not resolved by BPT.

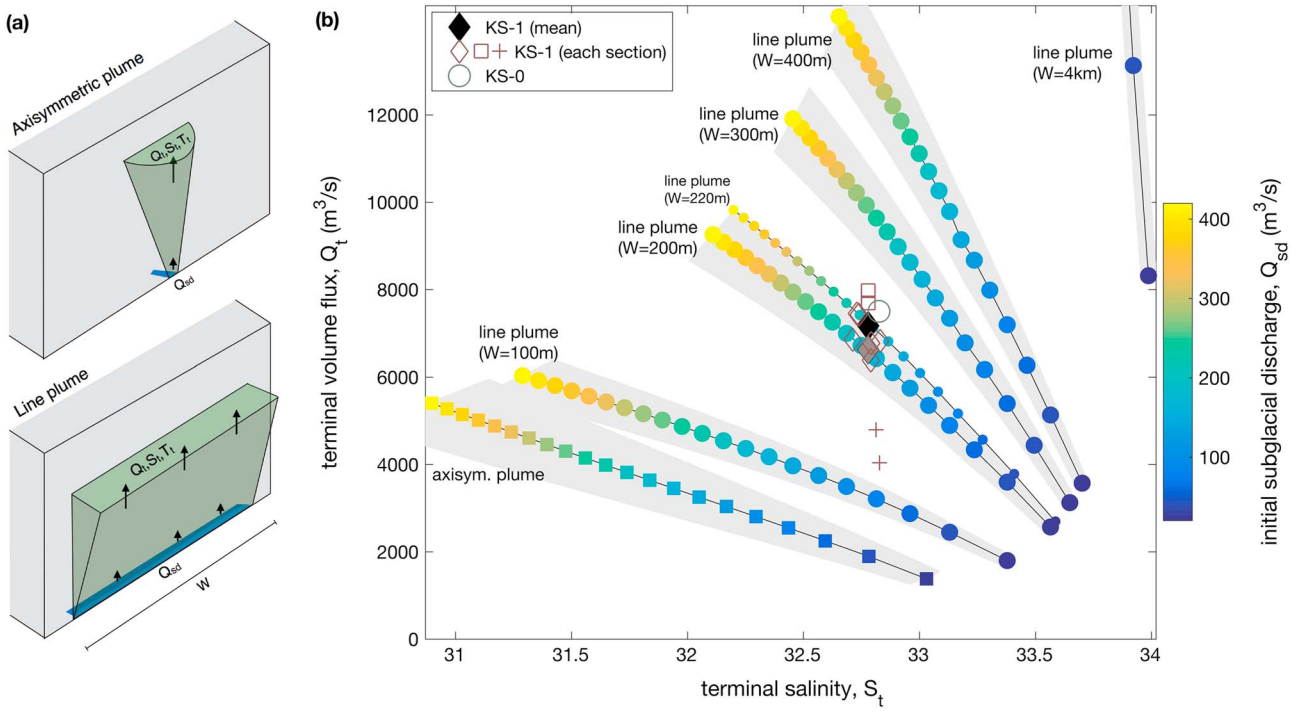

Figure 3. (a) Schematic of axisymmetric versus line plume theory. (b) Comparison of observed plume volume flux and salinity with the terminal properties from various versions of BPT. Each colored square shows the terminal volume flux and salinity of an axisymmetric BPT for a range of initial subglacial discharges (in 20 $m^3\ s^{-1}$ intervals of discharge), and colored circles are terminal properties from line BPT for the same range of discharges. Color indicates the subglacial discharge that initiates the plume. Brown symbols correspond to individual sections in Figure 1b. Grey-filled diamond is the mean of all sections. Black-filled diamond is the mean without the last two sections (crosses; separated by 7 h from the other sections). Grey circle is the KS-0 section. Grey shaded ranges for the BPT solutions are produced by varying the grounding line depth from 250 to 270 m and the entrainment coefficient from 0.09 to 0.11.

To compare axisymmetric BPT, line BPT, and the observations, we report all values in terms of total volume fluxes, e.g., 300 $m^3\ s^{-1}$ of discharge over a line plume of 200 m width would be input into the model as a discharge of 1.5 $m^2\ s^{-1}$, but the solution is then translated back into the total volume flux in $m^3\ s^{-1}$.

For each geometry of BPT, the terminal volume flux increases with the initial subglacial discharge, but, perhaps less intuitively, the terminal salinity decreases with higher discharge (Figure 3). Because the net entrainment scales sublinearly with the initial discharge, the ratio of entrained seawater to freshwater decreases with higher discharge, corresponding to a decrease in terminal salinity.

Axisymmetric BPT fails to match the observations for any subglacial discharge forcing (Figure 3). Low discharges in BPT have a lower terminal volume flux and higher terminal salinity (i.e., they equilibrate deeper in the water column), while higher discharges drive larger terminal volume fluxes and lower terminal salinities. The water properties of the observed plume match the axisymmetric solution for a low discharge of 40 $m^3\ s^{-1}$; however, this solution has a terminal volume flux that is less than a third of the observed volume flux (Figures 3 and S4). Similarly, axisymmetric theory for a high discharge of 500 $m^3\ s^{-1}$ replicates the observed volume flux, but the theoretical salinity is off by >2 psu, corresponding to more than a factor of 2 difference in dilution. This discrepancy between the observations and theory indicates that there must be more entrainment in the upwelling plume than axisymmetric BPT predicts.

Truncated line BPT solutions span a wide range of the parameter space in Figure 3, because entrainment scales with plume width, which is an adjustable parameter for the model. For a given flux of subglacial discharge, the terminal salinity and terminal volume flux increases as the line plume gets wider (Figure 3)—entrained volume flux per unit discharge increases as the plume surface area increases.

The best fit to the mean plume observations is a truncated line plume of 220 m width with 200 $m^3\ s^{-1}$ of initial discharge (Figure 3). Using the range of volume fluxes and salinities from the repeat sections, the plume width is 220 ± 20 m and the discharge 200 ± 40 $m^3\ s^{-1}$. Notably, this fitted line plume width is similar to the observed undercutting width (~200 m) at the terminus prow, where the plume originates [*Fried et al.*, 2015].

Additionally, the initial discharge in the best fit BPT solution is consistent with the upper limit of freshwater ($<260 \pm 70$ m^3 s^{-1}) and the rough estimate of subglacial discharge flux (190 ± 50 m^3 s^{-1}) from section 3.

We can also examine the terminal temperature and terminal height of the plume; however, these variables are somewhat extraneous as they do not provide additional constraints on the fit between theory and observations (supporting information).

5. Discussion

We have provided evidence that the standard axisymmetric BPT model cannot represent entrainment in the KS plume. Instead, two independent observations point toward a line plume of ~220 m width. First, multibeam sonar reveals a laterally confined, deeply undercut segment of terminus that is roughly 200 m wide, and the observed undercut presumably results from plume-enhanced submarine melting [*Fried et al.*, 2015]. For the full range of discharges considered here, the axisymmetric BPT solutions have initial radii of 4–16 m and terminal radii of 30–40 m—not broad enough to drive enhanced melting over a 200 m wide area. Second, the ocean observations of the plume's volume flux and water properties are consistent with a 220 m wide line plume forced by 200 m^3 s^{-1} of subglacial discharge and cannot match axisymmetric BPT with any initial discharge.

In addition to a 220 m wide line plume, there are other variations to BPT that could match the plume observations: (1) an axisymmetric plume with an entrainment coefficient (α) of 0.21, twice the typical value in the literature [e.g., *Morton et al.*, 1956; *Cowton et al.*, 2015; *Carroll et al.*, 2016]; (2) an axisymmetric plume initialized with subglacial discharge that is already diluted by a factor of 10, i.e., if there were intense mixing at the grounding line depth before the upwelling phase; or (3) four axisymmetric plumes that coalesce into one outflowing plume. All these scenarios involve entraining roughly 3 times more ambient water than the standard axisymmetric model. However, the truncated line plume model appears to be the simplest and most plausible scenario to explain the observations, given the geometry of the prow undercut.

Recent modeling studies typically use axisymmetric BPT to parameterize plumes from subglacial channels [e.g., *Kimura et al.*, 2014; *Slater et al.*, 2015; *Cowton et al.*, 2015; *Carroll et al.*, 2016; *Bartholomaus et al.*, 2016; *Cowton et al.*, 2016]; however, if these plumes actually behave more like truncated line plumes of $W = O(200\,\text{m})$, the entrainment, submarine melting, and freshwater dilution would be significantly enhanced. For example, 200 m^3 s^{-1} of subglacial discharge in KS as an axisymmetric plume would melt 0.6 m^3 s^{-1} and form a terminal plume of 3600 m^3 s^{-1} with 6% freshwater in the plume (supporting information). On the other hand, the same 200 m^3 s^{-1} discharge into KS as a line plume of 220 m width would melt 1.8 m^3 s^{-1} (3 times more) and form a terminal plume of 6500 m^3 s^{-1} with only 3% freshwater (twice the dilution). Additionally, the structure of the inflow toward the glacier is different: the entrained volume flux per unit depth will increase with height for the axisymmetric plume but decreases with height for the line plume (Figure S6). These are significant differences for modeling both the ocean's impact on the glacier via submarine melting and on the glacier's driving of fjord circulation.

In the axisymmetric versus line BPT comparison, both models use the same underlying physics and parameterizations of entrainment and melt. The difference in their solutions arises from their differences in geometry or, more specifically, the differences in their entraining surface area and in the ice surface area that has plume-enhanced submarine melt (supporting information Figure S6). Here we are not testing the underlying dynamics of plume theory, but instead, we are exploring what is the most appropriate geometry for modeling plumes from subglacial discharge channels with BPT.

Our results rely on the BPT entrainment parameterization being valid ($u_e = \alpha w$ where w is the vertical velocity and u_e the entrainment velocity), but they do not rely on the validity of the three-equation parameterization for melt [*Holland and Jenkins*, 1999]. This melt parameterization in the BPT model allows us to estimate melt rates, as in previous studies. However, in the parameter space of interest ($Q_{sg} \gg Q_m$), the contribution of melt to the plume's salinity and volume flux is effectively negligible; i.e., the plume's evolution affects the melt rate but the melt rate does not significantly affect the plume's evolution [*Carroll et al.*, 2015; *Cowton et al.*, 2015]. Thus, our results do not hinge on the unvalidated melt parameterizations.

In contrast to our results, *Mankoff et al.* [2016] state that their observations of a plume's volume flux and water properties in Saqqarliup glacier/fjord, Greenland, are roughly consistent with axisymmetric BPT. However, those observations differ by >1 psu in salinity from axisymmetric theory—a small error in terms

of the absolute salinity (~30) but almost a factor of 2 error in the plume dilution. When we apply the framework presented here to the Saqqarliup plume observations, we find that the Saqqarliup observations are best matched with a line plume of width 85±15 m (supporting information Figure S7), suggesting that the truncated line result from KS might be applicable more broadly.

Pointing in the same direction as our results, *Slater et al.* [2017a] argue that an observed plume (presumably emerging from a discharge channel) is inconsistent with axisymmetric theory and requires more distributed discharge with higher entrainment, based on surface observations from Kangiata Nunata Sermia in southwest Greenland.

While we primarily discuss the observations in terms of the plume geometry and terminus morphology, our results also have implications for the geometry of the subglacial discharge channel's outlet where it enters the fjord. Subglacial channels are often thought to be semicircular in shape (Rothlisberger, 1972), which is sometimes the explicit scaling used to initialize a discharge plume [*Xu et al.*, 2012; *Slater et al.*, 2015] and perhaps implicitly behind the general use of semicircular plume geometries with initial radii of $O(1-10$ m). However, there are no observations of this small and semicircular channel geometry at the termini of marine-terminating glaciers, and our observations here point toward a wider outlet that distributes the plume over ~200 m. However, we do not know how far upstream our results might be relevant to the channel geometry (e.g., the channel could fan out near the terminus).

This study leaves open several questions. First, we cannot address mixing in the plume's rebound and initial outflow. While our observed volume fluxes suggest limited entrainment between 500 m and 2 km from the glacier terminus, we cannot quantitatively constrain the entrainment between the overshoot and 500 m from the terminus. This uncertainty is an important caveat to our comparison between theory and observations, since BPT only models the upwelling portion of the plume. Additional entrainment in the rebound and initial horizontal outflow would increase the plume's volume flux and alter its water properties—though it is hard to predict how T/S would change since the subsurface plume can entrain from above, below, and laterally. Future studies are also needed to better resolve the deep inflow. The structure from the combined mooring and shipboard records shows local maxima in the inflow at ~70 m depth and also at the grounding line depth (Figure 2b). This profile does not match the entrainment profile for either a line or a axisymmetric plume (Figure S6).

Lastly, the shape of the undercut cavity might affect entrainment and melt, beyond what is represented with idealized BPT. At the sides of the plume, the cave-like shape of the undercut could inhibit entrainment and confine the plume width, while potentially enhancing melt by increasing the ice-plume surface area. It should also be noted that our results pertain to the primary plume at KS that emerges from the prow, but other smaller outlets along the terminus could generate plumes that behave differently.

6. Conclusions

With novel measurements of the near-glacier circulation, we have examined the 3-D structure of a subsurface plume that emerges from an undercut subglacial discharge outlet. When compared with idealized buoyant plume theory, the observations do not match the typical axisymmetric plume representation in models but instead suggest a truncated line plume of ~200 m width. This result is corroborated by independent observations of plume-enhanced melt over a 200 m wide undercut section of the glacier's terminus. Although plume theory is idealized, it is currently the primary (almost exclusive) tool for tuning or parameterizing plumes in numerical models. The truncated line plume proposed here would drive three times more melt and two times more entrainment than the most common parameterization of glacial plumes—significant differences for modeling ocean-driven melting and glacier-driven fjord circulation.

Acknowledgments
This project was primarily funded by the NASA grant NNX12AP50G. R. Jackson was funded by the NOAA Climate and Global Change postdoctoral fellowship. Data used in this work are available by emailing the corresponding author.

References

Bamber, J., M. van den Broeke, J. Ettema, J. Lenaerts, and E. Rignot (2012), Recent large increases in freshwater fluxes from Greenland into the North Atlantic, *Geophys. Res. Lett.*, *39*, L19501, doi:10.1029/2012GL052552.

Bartholomaus, T. C., et al. (2016), Contrasts in the response of adjacent fjords and glaciers to ice-sheet surface melt in West Greenland, *Ann. Glaciol.*, *57*(73), 25–38.

Beaird, N., F. Straneo, and W. Jenkins (2015), Spreading of Greenland meltwaters in the ocean revealed by noble gases, *Geophys. Res. Lett.*, *42*, 7705–7713, doi:10.1002/2015GL065003.

Bendtsen, J., J. Mortensen, K. Lennert, and S. Rysgaard (2015), Heat sources for glacial ice melt in a west Greenland tidewater outlet glacier fjord: The role of subglacial freshwater discharge, *Geophys. Res. Lett.*, *42*, 4089–4095, doi:10.1002/2015GL063846.

Carroll, D., D. A. Sutherland, E. L. Shroyer, J. D. Nash, G. A. Catania, and L. A. Stearns (2015), Modeling turbulent subglacial meltwater plumes: Implications for fjord-scale buoyancy-driven circulation, *J. Phys. Oceanogr.*, *45*, 2169–2185.
Carroll, D., D. Sutherland, and B. Hudson (2016), The impact of glacier geometry on meltwater plume structure and submarine melt in Greenland fjords, *Geophys. Res. Lett.*, *43*, 9739–9748, doi:10.1002/2016GL070170.
Cowton, T., D. Slater, A. Sole, D. Goldberg, and P. Nienow (2015), Modeling the impact of glacial runoff on fjord circulation and submarine melt rate using a new subgrid-scale parameterization for glacial plumes, *J. Geophys. Res. Oceans*, *120*, 796–812, doi:10.1002/2014JC010324.
Cowton, T., A. Sole, P. Nienow, D. Slater, D. Wilton, and E. Hanna (2016), Controls on the transport of oceanic heat to Kangerdlugssuaq Glacier, East Greenland, *J. Glaciol.*, *62*(236), 1167–1180.
Ellison, T. H., and J. S. Turner (1959), Turbulent entrainment in stratified flows, *J. Fluid Mech.*, *6*, 423–448.
Enderlin, E. M., I. M. Howat, S. Jeong, M.-J. Noh, J. H. Van Angelen, and M. R. van den Broeke (2014), An improved mass budget for the Greenland ice sheet, *Geophys. Res. Lett.*, *41*, 866–872, doi:10.1002/2013GL059010.
Fried, M. J., G. A. Catania, and T. C. Bartholomaus (2015), Distributed subglacial discharge drives significant submarine melt at a Greenland tidewater glacier, *Geophys. Res. Lett.*, *42*, 9328–9336, doi:10.1002/2015GL065806.
Gade, H. (1979), Melting of ice in sea water: A primitive model with application to the Antarctic ice shelf and icebergs, *J. Phys. Oceanogr.*, *9*(1), 189–198.
Holland, D. M., and A. Jenkins (1999), Modeling thermodynamic ice-ocean interactions at the base of an ice shelf, *J. Phys. Oceanogr.*, *29*(8), 1787–1800.
Holland, D. M., R. H. Thomas, B. de Young, M. H. Ribergaard, and B. Lyberth (2008), Acceleration of Jakobshavn Isbræ triggered by warm subsurface ocean waters, *Nat. Geosci.*, *1*(10), 659–664.
Jackson, R. H., and F. Straneo (2016), Heat, salt, and freshwater budgets for a glacial fjord in Greenland, *J. Phys. Oceanogr.*, *46*(9), 2735–2768.
Jenkins, A. (1999), The impact of melting ice on ocean waters, *J. Phys. Oceanogr.*, *29*(9), 2370–2381.
Jenkins, A. (2011), Convection-driven melting near the grounding lines of ice shelves and tidewater glaciers, *J. Phys. Oceanogr.*, *41*(12), 2279–2294.
Kimura, S., P. R. Holland, A. Jenkins, and M. Piggott (2014), The effect of meltwater plumes on the melting of a vertical glacier face, *J. Phys. Oceanogr.*, *44*, 3099–3117.
Lenaerts, J. T. M., D. Le Bars, L. Kampenhout, M. Vizcaino, E. M. Enderlin, and M. R. Broeke (2015), Representing Greenland ice sheet freshwater fluxes in climate models, *Geophys. Res. Lett.*, *42*, 6373–6381, doi:10.1002/2015GL064738.
MacAyeal, D. R. (1985), Evolution of tidally triggered meltwater plumes below ice shelves, in *Oceanology of the Antarctic Continental Shelf*, edited by S. S. Jacobs, pp. 133–143, AGU, Washington, D. C.
Mankoff, K. D., F. Straneo, C. Cenedese, S. B. Das, C. G. Richards, and H. Singh (2016), Structure and dynamics of a subglacial discharge plume in a Greenlandic fjord, *J. Geophys. Res. Oceans*, *121*, 8670–8688, doi:10.1002/2016JC011764.
Morton, B. R., G. Taylor, and J. S. Turner (1956), Turbulent gravitational convection from maintained and instantaneous sources, *Proc. R. Soc. A*, *234*(1196), 1–23.
Motyka, R., L. Hunter, K. Echelmeyer, and C. Connor (2003), Submarine melting at the terminus of a temperate tidewater glacier, LeConte Glacier, Alaska, USA, *Ann. Glaciol.*, *36*, 57–65.
Motyka, R. J., M. Truffer, M. Fahnestock, J. Mortensen, S. Rysgaard, and I. Howat (2011), Submarine melting of the 1985 Jakobshavn Isbræ floating tongue and the triggering of the current retreat, *J. Geophys. Res.*, *116*, F01007, doi:10.1029/2009JF001632.
Noel, B., W. J. van de Berg, E. van Meijgaard, P. Kuipers Munneke, R. S. W. van de Wal, and M. R. van den Broeke (2015), Evaluation of the updated regional climate model RACMO2.3: Summer snowfall impact on the Greenland Ice Sheet, *Cryosphere*, *9*(5), 1831–1844.
Sciascia, R., F. Straneo, C. Cenedese, and P. Heimbach (2013), Seasonal variability of submarine melt rate and circulation in an East Greenland fjord, *J. Geophys. Res. Oceans*, *118*, 2492–2506, doi:10.1002/jgrc.20142.
Shepherd, A., et al. (2012), A reconciled estimate of ice-sheet mass balance, *Science*, *338*(6111), 1183–1189.
Slater, D., P. W. Nienow, and T. R. Cowton (2015), Effect of near-terminus subglacial hydrology on tidewater glacier submarine melt rates, *Geophys. Res. Lett.*, *42*, 2861–2868, doi:10.1002/2014GL062494.
Slater, D., D. N. Goldberg, P. W. Nienow, and T. R. Cowton (2016), Scalings for submarine melting at tidewater glaciers from buoyant plume theory, *J. Phys. Oceanogr.*, *46*, 1839–1855.
Slater, D., P. Nienow, A. Sole, T. Cowton, R. Mottram, P. Langen, and D. Mair (2017a), Spatially distributed runoff at the grounding line of a large Greenlandic tidewater glacier inferred from plume modelling, *J. Glaciol.*, *63*, 309–323.
Slater, D., P. W. Nienow, D. N. Goldberg, T. R. Cowton, and A. J. Sole (2017b), A model for tidewater glacier undercutting by submarine melting, *Geophys. Res. Lett.*, *44*, 2360–2368, doi:10.1002/2016GL072374.
Stevens, L. A., F. Straneo, S. B. Das, A. J. Plueddemann, A. L. Kukulya, and M. Morlighem (2016), Linking glacially modified waters to catchment-scale subglacial discharge using autonomous underwater vehicle observations, *Cryosphere*, *10*(1), 417–432.
Straneo, F., and P. Heimbach (2013), North Atlantic warming and the retreat of Greenland's outlet glaciers, *Nat. Commun.*, *504*(7478), 36–43.
Weijer, W., M. E. Maltrud, M. W. Hecht, H. A. Dijkstra, and M. A. Kliphuis (2012), Response of the Atlantic Ocean circulation to Greenland Ice Sheet melting in a strongly-eddying ocean model, *Geophys. Res. Lett.*, *39*(L09606), doi:10.1029/2012GL051611.
Xu, Y., E. Rignot, D. Menemenlis, and M. Koppes (2012), Numerical experiments on subaqueous melting of Greenland tidewater glaciers in response to ocean warming and enhanced subglacial discharge, *Ann. Glaciol.*, *53*(60), 229–234.